

Revisiting particle circular orbits as probes of black hole thermodynamics

Lei You^{1,*} and Jinsong Yang^{1,†}

¹*School of Physics, Guizhou University, Guiyang 550025, China*

Recent studies propose that black hole phase transitions can be encoded in the circular orbit radius of particles. In this paper, we systematically investigate the reliability of this encoding mechanism. We find that this mechanism is highly reliable in the isobaric ensemble, whereas it may break down in the isothermal ensemble. It turns out that the reliability of this mechanism is directly controlled by the first law of black hole thermodynamics. Interestingly, even if this encoding mechanism fails, we prove that, for any black hole exhibiting criticality, the first law can ensure that, near the critical point, the coexistence gap of the circular orbit radius remains a reliable order parameter and yields exactly the same critical exponents as the standard thermodynamic order parameter. Our results provide a potential way to identify the thermodynamic ensemble of a black hole, and reveal a deeper connection between gravitational geometry and thermodynamics.

I. INTRODUCTION

Black hole thermodynamics provides a unique arena for exploring the interplay among gravity, quantum physics, and statistical mechanics. It began as a formal analogy between the laws of black hole mechanics and ordinary thermodynamics, and acquired genuine physical content through the generalized second law and Hawking radiation [1–4]. Subsequent developments connected it to broader areas of physics, for example microscopic state counting in string theory and holography in AdS/CFT [5–7]. Particularly influential progress has come from AdS black holes in the extended phase space, where the cosmological constant is interpreted as a pressure and the mass as an enthalpy. Within this framework, AdS black holes were found to possess a rich phase structure, including Van der Waals-like phase transitions and criticality, as well as more exotic behaviors in modified gravity and nonlinear electrodynamics [8–16].

These advances further confirm that black hole thermodynamics carries genuine physical content and naturally raise the question how it can be tested. A particularly compelling possibility comes from horizon-scale imaging. The Event Horizon Telescope has imaged the shadows of the supermassive black holes in M87 and at the Galactic center, opening a new observational window on strong-field optical phenomena [17, 18]. Motivated by this breakthrough, recent theoretical work has begun to explore how thermodynamic phase transitions may leave imprints on optical observables. In particular, Wei *et al.* showed that in the isobaric ensemble the photon sphere radius can serve as an effective probe of the small-/large-black hole phase transition, suggesting that thermodynamic evolution may be reflected in observable image features [19, 20]. Subsequently, related signatures involving photon spheres and innermost stable circular orbits (ISCOs) have been identified across a variety of spacetimes and modified theories of gravity [21–24].

A key ingredient in these studies is the monotonicity of the mapping between the circular orbit radius r_c and the horizon radius r_h . Across a first-order small/large phase transition, r_h

undergoes a discontinuous jump, and the monotonic mapping $r_c(r_h)$ ensures that r_c also jumps accordingly, thereby making r_c a natural geometric order parameter (see Appendix A for a brief mathematical derivation). This expectation was later formalized by Zhang *et al.*, who proved a monotonic increase of the photon sphere and ISCO radii with r_h in general static, spherically symmetric geometries, and this result has been widely adopted in subsequent work [25, 26].

However, we find that once more than one thermodynamic parameter is allowed to vary, the claim of monotonic increase may fail. To illustrate this, we present a simple counterexample based on the Schwarzschild–AdS (Sch–AdS) black hole: the photon sphere radius $r_{ps} = 3M$ depends only on the mass M , whereas the horizon radius r_h depends on both M and the pressure $P = -\Lambda/(8\pi)$ associated with the negative cosmological constant Λ . Increasing P decreases r_h , with r_{ps} unchanged. Consequently, there exist smooth paths in (M, P) parameter space along which r_h increases and r_{ps} decreases. Figure 1 provides an explicit path example, and Appendix B presents an analytic example by constructing an explicit parametric path. This breakdown of monotonic increase in $r_c(r_h)$ has been neglected in previous studies, and the reason is straightforward: Most analyses have been restricted to the isobaric ensemble, where P is held fixed and only M varies, resulting in both r_c and r_h typically increasing monotonically with M . Even when isothermal ensembles were considered (with both M and P varying), the monotonicity of $r_c(r_h)$ was not examined systematically, so possible monotonic decrease or nonmonotonicity was overlooked. Thus, understanding how circular orbits encode black hole phase transitions and other thermodynamic information calls for analyzing the monotonicity of $r_c(r_h)$ along general parameter paths, which is precisely the focus of this work.

Our strategy is as follows. In Sec. II, we review the conditions for the photon sphere and the ISCO in a general static, spherically symmetric spacetime and derive a unified expression for dr_c/dr_h along an arbitrary path in parameter space. In Sec. III, we analyze the monotonicity of $r_c(r_h)$ for d -dimensional Reissner–Nordström–AdS (RN–AdS) black holes, focusing on isobaric and isothermal thermodynamic paths. In Sec. IV, we show that the critical exponents are invariant under the reparametrization $r_h \mapsto r_c$, so that r_c and r_h yield the same universality class. Finally, Sec. V summarizes

* gs.lyou25@gzu.edu.cn

† Corresponding author: jsyang@gzu.edu.cn

and discusses our main results. Throughout this work we employ natural units with $c = G = 1$.

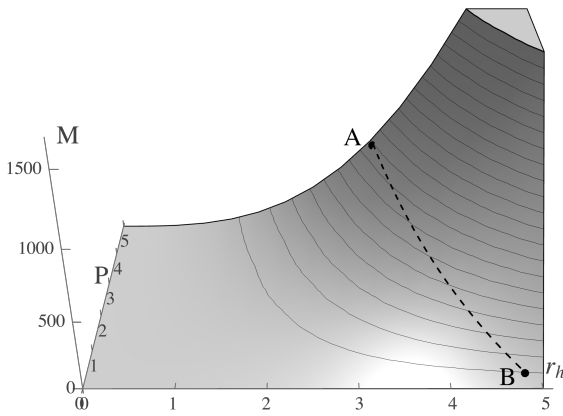


FIG. 1. Behavior of $M(r_h, P)$ in the Sch–AdS spacetime. Thin black solid curves denote contours of constant mass M . Along the dashed trajectory from A to B, the horizon radius r_h increases while both M and the photon sphere radius $r_{\text{ps}} = 3M$ decrease, showing that $r_{\text{ps}}(r_h)$ is strictly monotonically decreasing along this path.

II. MONOTONICITY CRITERION

A. Review of circular orbits

Consider a static, spherically symmetric spacetime with the line element

$$ds^2 = -f(r; \lambda) dt^2 + \frac{dr^2}{f(r; \lambda)} + r^2 d\Omega^2, \quad (2.1)$$

where $f(r; \lambda)$ is a smooth function of the radial coordinate r , while $\lambda = (\lambda_1, \dots, \lambda_n)$ denotes the set of black hole parameters, such as mass M , charge q , and so on. The Lagrangian of a particle moving in the spacetime determined by Eq. (2.1) reads

$$\mathcal{L} = \frac{1}{2} g_{\mu\nu} \dot{x}^\mu \dot{x}^\nu = -\frac{1}{2} \epsilon, \quad \epsilon = \begin{cases} 0, & \text{massless particle (photon),} \\ 1, & \text{massive particle.} \end{cases} \quad (2.2)$$

Where the overdot denotes differentiation with respect to the affine parameter. Without loss of generality, we set $\theta = \pi/2$, restricting the motion to the equatorial plane. Then, the Lagrangian reduces to

$$\mathcal{L} = \frac{1}{2} \left[-f(r; \lambda) \dot{t}^2 + \frac{\dot{r}^2}{f(r; \lambda)} + r^2 \dot{\phi}^2 \right] = -\frac{1}{2} \epsilon. \quad (2.3)$$

Since the metric is stationary and axisymmetric, the corresponding cyclic coordinates t and ϕ give rise to two conserved quantities,

$$E := -\frac{\partial \mathcal{L}}{\partial \dot{t}} = f(r; \lambda) \dot{t}, \quad L := \frac{\partial \mathcal{L}}{\partial \dot{\phi}} = r^2 \dot{\phi}, \quad (2.4)$$

which represent the particle's energy and angular momentum, respectively. Substituting Eq. (2.4) into Eq. (2.3) yields the following radial equation of motion

$$\dot{r}^2 = E^2 - f(r) \left(\epsilon + \frac{L^2}{r^2} \right) \equiv \mathcal{R}(r). \quad (2.5)$$

The particle's circular orbits at $r = r_c$ are determined by

$$\mathcal{R}(r_c) = 0, \quad \mathcal{R}'(r_c) = 0, \quad (2.6)$$

where the prime denotes differentiation with respect to r .

Solving Eq. (2.6) for a massless particle with $\epsilon = 0$ gives (see Appendix C for a detailed derivation)

$$\Phi_0(r; \lambda) := r \partial_r f(r; \lambda) - 2f(r; \lambda) = 0, \quad \text{at } r = r_{\text{ps}}, \quad (2.7)$$

where r_{ps} denotes the photon sphere radius. The condition for an unstable photon sphere further requires

$$\mathcal{R}''(r_{\text{ps}}) > 0, \quad (2.8)$$

which is equivalent to

$$\Gamma_0(\lambda) := \partial_r \Phi_0(r; \lambda)|_{r_{\text{ps}}} < 0. \quad (2.9)$$

The ISCO of a massive particle with $\epsilon = 1$ marks the transition between stable and unstable circular motion and is defined by the marginal stability condition

$$\mathcal{R}(r_{\text{isco}}) = \mathcal{R}'(r_{\text{isco}}) = \mathcal{R}''(r_{\text{isco}}) = 0, \quad (2.10)$$

which can be recast into a universal form,

$$\Phi_1(r; \lambda) := r f(r; \lambda) \partial_r^2 f(r; \lambda) - 2r(\partial_r f(r; \lambda))^2 + 3f(r; \lambda) \partial_r f(r; \lambda) = 0, \quad \text{at } r = r_{\text{isco}}. \quad (2.11)$$

To ensure that circular orbits are stable outside ISCO but unstable inside, one further requires its radius r_{isco} to satisfy

$$\Gamma_1(\lambda) := \partial_r \Phi_1(r; \lambda)|_{r_{\text{isco}}} > 0. \quad (2.12)$$

Summarizing the above conditions, we have

$$\Phi_\epsilon(r; \lambda) = 0, \quad \text{at } r = r_c(\epsilon; \lambda) := \begin{cases} r_{\text{ps}}(\lambda), & \epsilon = 0, \\ r_{\text{isco}}(\lambda), & \epsilon = 1, \end{cases} \quad (2.13)$$

and the corresponding stability criteria

$$\Gamma_\epsilon \begin{cases} < 0, & \epsilon = 0, \\ > 0, & \epsilon = 1. \end{cases} \quad (2.14)$$

B. Derivation of the Monotonicity Criterion

To investigate the monotonic relation between the circular orbit radius r_c and the event-horizon radius r_h , we first express them in terms of the previously defined functions $\Phi_\epsilon(r; \lambda)$ and $f(r; \lambda)$

$$\Phi_\epsilon(r_c; \lambda) = 0, \quad f(r_h; \lambda) = 0. \quad (2.15)$$

According to the implicit function theorem, if

$$\partial_r \Phi_\epsilon|_{(r_c; \lambda)} \neq 0, \quad \partial_r f|_{(r_h; \lambda)} \neq 0, \quad (2.16)$$

then there exist locally smooth functions $r_c(\lambda)$ and $r_h(\lambda)$ in the neighborhoods of $(r_c; \lambda)$ and $(r_h; \lambda)$, respectively. Fortunately, according to Eqs. (2.9) and (2.12), one finds

$$\partial_r \Phi_\epsilon|_{(r_c; \lambda)} = \Gamma_\epsilon \neq 0, \quad (2.17)$$

and

$$\partial_r f|_{(r_h; \lambda)} = 2\kappa \neq 0, \quad (2.18)$$

where $\kappa = \frac{1}{2} \partial_r f(r; \lambda)|_{(r_h; \lambda)}$ is the surface gravity of the black hole, which is positive for any nonextremal case. Hence, the conditions (2.16) are automatically satisfied.

Based on this, Eq. (2.15) can in principle be differentiated with respect to λ . Since the parameter set λ generally contains several components, it is convenient to introduce a smooth path $\lambda(\tau)$ in the parameter space, along which all quantities become functions of a single real variable τ . This allows us to directly apply the chain rule, yielding

$$\frac{d}{d\tau} \Phi_\epsilon(r_c(\tau); \lambda(\tau)) = \partial_{r_c} \Phi_\epsilon \dot{r}_c + \langle \nabla_\lambda \Phi_\epsilon, \dot{\lambda} \rangle = 0, \quad (2.19)$$

$$\frac{d}{d\tau} f(r_h(\tau); \lambda(\tau)) = \partial_{r_h} f \dot{r}_h + \langle \nabla_\lambda f, \dot{\lambda} \rangle = 0, \quad (2.20)$$

where the overdot denotes differentiation with respect to τ , and $\langle \nabla_\lambda F, \dot{\lambda} \rangle \equiv \sum_{i=1}^n (\partial_{\lambda_i} F) \dot{\lambda}_i$. Combining Eqs. (2.19) and (2.20), we finally obtain

$$\frac{dr_c}{dr_h} = \frac{\dot{r}_c}{\dot{r}_h} = \frac{2\kappa}{\Gamma_\epsilon} \frac{\langle \nabla_\lambda \Phi_\epsilon, \dot{\lambda} \rangle}{\langle \nabla_\lambda f, \dot{\lambda} \rangle}, \quad (\dot{r}_h \neq 0), \quad (2.21)$$

where we have written Φ_ϵ and f as shorthand for $\Phi_\epsilon(r_c; \lambda)$ and $f(r_h; \lambda)$, respectively, and this convention will be used throughout the paper.

The criterion (2.21) shows that the monotonic relation between r_c and r_h is governed by two independent factors. The first factor, $2\kappa/\Gamma_\epsilon$, is purely geometric, determined by the intrinsic properties of the black hole and its circular orbits. As discussed earlier, it remains nonvanishing and therefore does not affect the monotonicity of $r_c(r_h)$. The second factor, $\langle \nabla_\lambda \Phi_\epsilon, \dot{\lambda} \rangle / \langle \nabla_\lambda f, \dot{\lambda} \rangle$, encodes how the parameters evolve along a chosen path in the thermodynamic space. It therefore determines whether the overall monotonicity of $r_c(r_h)$ is preserved or violated, emphasizing the importance of considering multiparameter constraints in black hole thermodynamics, as discussed in the Introduction.

In the next section, we apply the criterion (2.21) to two physically relevant constraints in black hole thermodynamics, namely the isobaric and isothermal processes, and investigate the monotonicity of $r_c(r_h)$ for the d -dimensional RN-AdS black hole.

III. EXAMPLES OF d -DIMENSIONAL BLACK HOLES UNDER ISOBARIC AND ISOTHERMAL CONSTRAINTS

In d -dimensional spacetime, a static and spherically symmetric AdS black hole is described by the line element

$$ds^2 = -f(r) dt^2 + \frac{dr^2}{f(r)} + r^2 d\Omega_{d-2}^2, \quad (3.1)$$

where $d\Omega_{d-2}^2$ denotes the line element of a unit $(d-2)$ -sphere. The metric function takes the general form

$$f(r) = 1 - \frac{c_d M}{r^{d-3}} + \frac{q^2}{r^{2(d-3)}} + \frac{16\pi P}{(d-1)(d-2)} r^2, \quad (3.2)$$

where M is the ADM mass, q is the charge parameter, and $P = -\Lambda/(8\pi)$ represents the thermodynamic pressure associated with the cosmological constant Λ . The coefficients

$$c_d = \frac{16\pi}{(d-2)\Omega_{d-2}}, \quad \Omega_{d-2} = \frac{2\pi^{(d-1)/2}}{\Gamma((d-1)/2)}, \quad (3.3)$$

depend only on the spacetime dimension, with Ω_{d-2} being the area of the unit $(d-2)$ -sphere. The metric (3.2) reproduces several well-known limits:

- $q = 0$: the d -dimensional Sch–AdS black hole;
- $q \neq 0$: the RN–AdS black hole;
- $P \rightarrow 0$: the asymptotically flat Schwarzschild or RN solution in d dimensions.

A. Isobaric Process

The isobaric process corresponds to the T – S ensemble commonly employed in black hole thermodynamics. Here, all thermodynamic variables except the mass remain fixed. Thus, we may take $\lambda = (M; \lambda_{\text{fixed}})$ and choose M itself as the path parameter. This leads to $\dot{r}_h = dr_h/dM$. To examine whether \dot{r}_h can vanish, we consider the first law of black hole thermodynamics

$$dM = T dS \quad \Rightarrow \quad \frac{dr_h}{dM} = \frac{1}{T S'(r_h)}, \quad (3.4)$$

where $T = 2\kappa/4\pi = \partial_r f(r; \lambda)/4\pi|_{(r_h; \lambda)} > 0$ is the Hawking temperature, and $S'(r_h) = dS/dr_h$. In d -dimensional general relativity, $S = A/4$ with $A = \Omega_{d-2} r_h^{d-2} > 0$, so that

$$S'(r_h) = \frac{\Omega_{d-2}}{4} (d-2) r_h^{d-3} > 0 \quad \Rightarrow \quad \frac{dr_h}{dM} > 0. \quad (3.5)$$

Hence, taking M as the path parameter is fully justified, and the general criterion (2.21) simplifies to

$$\frac{dr_c}{dr_h} = -\frac{1}{\Gamma_\epsilon} \frac{dM}{dr_h} \partial_M \Phi_\epsilon. \quad (3.6)$$

The monotonicity of $r_c(r_h)$ is therefore governed by $\partial_M \Phi_\epsilon$. Although no fundamental law requires $\partial_M \Phi_\epsilon \neq 0$, the mass M

fixes the background geometry and thus controls the circular orbits, so they generically vary with M . Based on this consideration and the universality of the first law, we expect that for almost all black holes the mapping $r_c(r_h)$ is monotonic in the isobaric ensemble. As a result, when a phase transition drives the horizon radius to jump from the small-black hole branch $r_{h,s}$ to the large-black hole branch $r_{h,l}$, the circular orbit radius undergoes a corresponding jump from $r_c(r_{h,s})$ to $r_c(r_{h,l})$. This makes the circular orbit radius a robust and reliable encoder of the phase transition information.

For the metric (3.2), we obtain

$$\begin{aligned}\partial_M \Phi_0 &= (d-1) \frac{c_d}{r_{\text{ps}}^{d-3}} > 0, \\ \partial_M \Phi_1 &= -\frac{2r_{\text{isco}}^{1-4d}}{(d-1)(d-2)} \sqrt{h(r_{\text{isco}}, q, P, d)} < 0,\end{aligned}\quad (3.7)$$

where the explicit expression of h is omitted for brevity. Substituting Eq. (3.7) into the criterion (3.6) and using Eqs. (2.14) and (3.5), we find

$$\epsilon = 0 : -\frac{1}{\Gamma_0} \frac{dM}{dr_h} > 0, \quad \partial_M \Phi_0 > 0 \Rightarrow \frac{dr_{\text{ps}}}{dr_h} > 0, \quad (3.8)$$

$$\epsilon = 1 : -\frac{1}{\Gamma_1} \frac{dM}{dr_h} < 0, \quad \partial_M \Phi_1 < 0 \Rightarrow \frac{dr_{\text{isco}}}{dr_h} > 0. \quad (3.9)$$

Hence, along an isobaric process, both $r_{\text{ps}}(r_h)$ and $r_{\text{isco}}(r_h)$ increase monotonically. The opposite signs of Γ_0 and Γ_1 are exactly compensated by those of $\partial_M \Phi_0$ and $\partial_M \Phi_1$, resulting in a consistent monotonic relation between r_c and r_h . These findings are consistent with the earlier results reported by Wei, Zhang, *et al.*

Next, we take $d = 4$ as an explicit example and compute the expression of dr_c/dr_h . For the four-dimensional RN-AdS black hole, one obtains

$$\begin{aligned}\frac{dM}{dr_h} &= \frac{2\kappa}{c_d/r_h^{d-3}} = \frac{2(-q^2/r_h^3 + 1/r_h + 8\pi P r_h)}{c_d/r_h^{d-3}} > 0, \\ \Gamma_0 &= \frac{4q^2 - 2r_{\text{ps}}^2}{r_{\text{ps}}^3} < 0, \\ \Gamma_1 &= \frac{1}{6r_{\text{isco}}^6} \left[15q^4 + r_{\text{isco}}^4 + 352\pi P r_{\text{isco}}^6 + 4800\pi^2 P^2 r_{\text{isco}}^8 \right. \\ &\quad + r_{\text{isco}}^2 \sqrt{g} - 120\pi P r_{\text{isco}}^4 \sqrt{g} \\ &\quad \left. + q^2(48\pi P r_{\text{isco}}^4 - 9\sqrt{g}) \right] > 0,\end{aligned}\quad (3.10)$$

where

$$\begin{aligned}g &= -15q^4 + r_{\text{isco}}^4 + 176\pi P r_{\text{isco}}^6 \\ &\quad + 1600\pi^2 P^2 r_{\text{isco}}^8 + 6q^2 r_{\text{isco}}^2 (3 + 8\pi P r_{\text{isco}}^2).\end{aligned}\quad (3.11)$$

It is straightforward to verify that the expression of dM/dr_h here is consistent with that given in Eq. (3.4). Using the criterion (3.6) together with the above results, we find

$$\frac{dr_{\text{ps}}}{dr_h} = \frac{3r_{\text{ps}}^2(q^2 - r_h^2 - 8\pi P r_h^4)}{2(2q^2 - r_{\text{ps}}^2)r_h^2}, \quad (3.12)$$

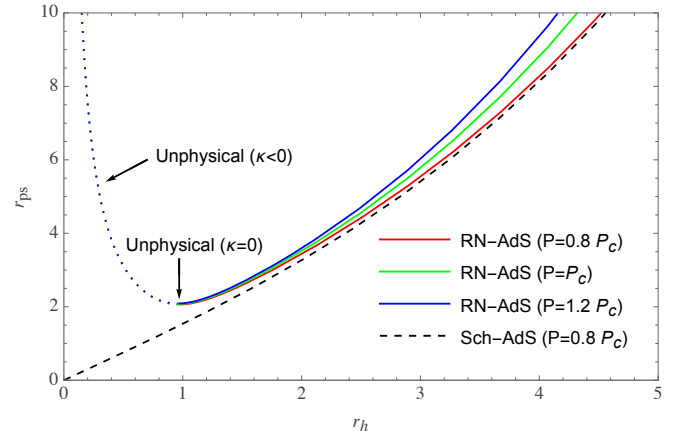


FIG. 2. Behavior of $r_{\text{ps}}(r_h)$ along isobaric paths in $d = 4$. For the Sch-AdS case, the pressure is likewise set to the value $P = 0.8 P_c$, where P_c is the critical pressure of the RN-AdS solution with $q = 1$. The same choice is adopted for subsequent figures and will not be restated hereafter.

and

$$\begin{aligned}\frac{dr_{\text{isco}}}{dr_h} &= -6(q^2 - r_h^2 - 8\pi P r_h^4) r_{\text{isco}}^{13} \sqrt{g} / \\ &\quad \left[r_h^2 (15q^4 r_{\text{isco}}^{11} + r_{\text{isco}}^{15} + 352\pi P r_{\text{isco}}^{17} + 4800\pi^2 P^2 r_{\text{isco}}^{19} \right. \\ &\quad \left. + 48\pi P q^2 r_{\text{isco}}^{15} + (r_{\text{isco}}^2 - 120\pi P r_{\text{isco}}^4 - 9q^2) r_{\text{isco}}^{11} \sqrt{g}) \right].\end{aligned}\quad (3.13)$$

In the Sch-AdS limit ($q = 0$), the above relations reduce to

$$\frac{dr_{\text{ps}}}{dr_h} = \frac{3}{2} + 12\pi P r_h^2, \quad (3.14)$$

$$\begin{aligned}\frac{dr_{\text{isco}}}{dr_h} &= 6(1 + 8\pi P r_h^2) \sqrt{j} / \left[1 + 4800\pi^2 P^2 r_{\text{isco}}^4 + \sqrt{j} \right. \\ &\quad \left. - 8\pi P r_{\text{isco}}^2 (-44 + 15\sqrt{j}) \right],\end{aligned}\quad (3.15)$$

where $j = 1 + 176\pi P r_{\text{isco}}^2 + 1600\pi^2 P^2 r_{\text{isco}}^4$. Further, in the limit where both q and P approach zero, one obtains

$$\frac{dr_{\text{ps}}}{dr_h} = \frac{3}{2}, \quad \frac{dr_{\text{isco}}}{dr_h} = 3, \quad (3.16)$$

which are consistent with the well-known relations $r_{\text{ps}} = 3M$, $r_{\text{isco}} = 6M$, and $r_h = 2M$ in the Schwarzschild case.

In Figs. 2 and 3, we present the numerically computed profiles of $r_{\text{ps}}(r_h)$ and $r_{\text{isco}}(r_h)$ for the four-dimensional case. In both panels, P_c denotes the pressure at the RN-AdS critical point, obtained from the criticality conditions $\partial T/\partial r_h = \partial^2 T/\partial r_h^2 = 0$. As illustrated, $r_c(r_h)$ remains globally monotonic for the Sch-AdS black hole, whereas for the RN-AdS black hole, it first decreases and then increases, with the extremum exactly at the point where $dM/dr_h = \kappa = 0$. Truncating the curve at this point, $r_c(r_h)$ retains its local monotonicity. These numerical results are in complete agreement with Eqs. (3.12)–(3.15).

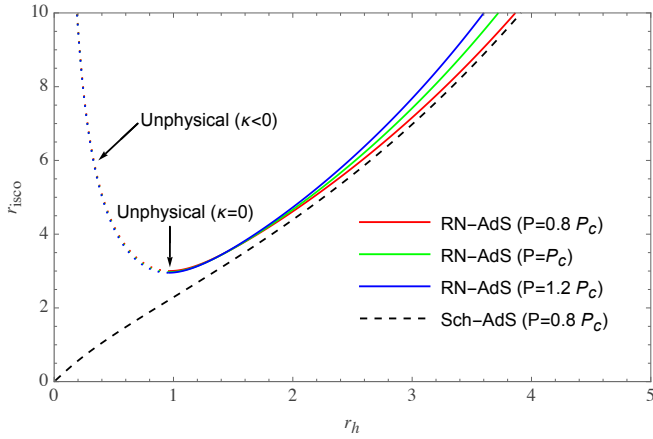


FIG. 3. Behavior of $r_{\text{isco}}(r_h)$ along isobaric paths in $d = 4$

B. Isothermal Process

The isothermal process corresponds to the P - V ensemble commonly employed in black hole thermodynamics. Here, the only variable parameters are M and P , which are related through the isothermal constraint $T(r_h; M, P) = T_0$. Therefore, we take $\lambda = (M, P; \lambda_{\text{fixed}})$. Substituting this into the criterion (2.21) and choosing r_h as the path parameter yields the following result [see Appendix D for justification of the existences of $M(r_h)$ and $P(r_h)$]

$$\frac{dr_c}{dr_h} = -\frac{1}{\Gamma_\epsilon} \left(\frac{dM}{dr_h} \partial_M \Phi_\epsilon + \frac{dP}{dr_h} \partial_P \Phi_\epsilon \right). \quad (3.17)$$

In general, this relation has no simple closed form. However, for photons ($\epsilon = 0$), many black hole metrics satisfy $\partial_P \Phi_0 = 0$, e.g., when the pressure enters the metric only through a term proportional to $P r^2$. In such cases, the criterion (3.17) reduces to

$$\frac{dr_{\text{ps}}}{dr_h} = -\frac{1}{\Gamma_0} \frac{dM}{dr_h} \partial_M \Phi_0. \quad (3.18)$$

This result is consistent with the criterion for the isobaric process, but differs in that the isobaric constraint requires $dM/dr_h > 0$ via the first law, ensuring the monotonicity of $r_{\text{ps}}(r_h)$. In contrast, under the isothermal constraint, the first law takes the form

$$dM = T_0 dS + V dP, \quad (3.19)$$

where V is the thermodynamic volume. Dividing both sides by dr_h yields

$$\frac{dM}{dr_h} = T_0 S'(r_h) + V \frac{dP}{dr_h}, \quad (3.20)$$

indicating that dM/dr_h may vanish or even become negative, which in turn allows $r_{\text{ps}}(r_h)$ to become nonmonotonic. This behavior is physically intuitive: when $dM/dr_h = 0$, one must have

$$\frac{dP}{dr_h} = -\frac{T_0}{V} S'(r_h) < 0. \quad (3.21)$$

This means that, near an extremum of $M(r_h)$, the same M corresponds to two distinct P . Since r_{ps} is P -independent (since $\partial_P \Phi_0 = 0$) while r_h depends on P , a single r_{ps} maps to two different r_h , and thus $r_{\text{ps}}(r_h)$ is necessarily nonmonotonic.

For massive particles ($\epsilon = 1$), one typically has $\partial_P \Phi_1 \neq 0$. Taking into account that M and P usually affect r_{isco} in opposite ways, we assume that $\partial_M \Phi_1$ and $\partial_P \Phi_1$ carry opposite signs (as is indeed the case for RN-AdS black holes). Under this assumption, the criterion (3.17) shows that if dM/dr_h and dP/dr_h have opposite signs, then dr_{isco}/dr_h cannot cross zero, so $r_{\text{isco}}(r_h)$ remains monotonic. Conversely, if dM/dr_h and dP/dr_h share the same sign, dr_{isco}/dr_h can in principle vanish, leading to a nonmonotonic $r_{\text{isco}}(r_h)$. Interestingly, the first law naturally allows for such nonmonotonic behavior: from Eq. (3.20) one sees that $dP/dr_h > 0$ implies $dM/dr_h > 0$, while $dM/dr_h < 0$ implies $dP/dr_h < 0$, so there exist regimes where dM/dr_h and dP/dr_h have the same sign and $r_{\text{isco}}(r_h)$ can become nonmonotonic.

Conversely, if we assume that $\partial_M \Phi_1$ and $\partial_P \Phi_1$ share the same sign, the first law will require that $r_{\text{isco}}(r_h)$ be nonmonotonic. The reason is simple: At an extremum of $M(r_h)$, one has $dM/dr_h = 0$, and thus Eq. (3.20) requires $dP/dr_h < 0$. Substituting these relations into the criterion (3.17) yields

$$\text{sgn}\left(\frac{dr_{\text{isco}}}{dr_h}\right) \Big|_{dM/dr_h=0} = \text{sgn}\left(-\frac{1}{\Gamma_1} \frac{dP}{dr_h} \partial_P \Phi_1\right). \quad (3.22)$$

At an extremum of $P(r_h)$, one instead has $dP/dr_h = 0$, and thus Eq. (3.20) gives $dM/dr_h > 0$. Inserting this into the criterion (3.17) leads to

$$\text{sgn}\left(\frac{dr_{\text{isco}}}{dr_h}\right) \Big|_{dP/dr_h=0} = \text{sgn}\left(-\frac{1}{\Gamma_1} \frac{dM}{dr_h} \partial_M \Phi_1\right). \quad (3.23)$$

It is easy to see that the two above expressions have different signatures. Therefore, the first law enforces a sign change in dr_{isco}/dr_h , implying that $r_{\text{isco}}(r_h)$ is necessarily nonmonotonic, with its extremum located between those of $M(r_h)$ and $P(r_h)$. Whether such a configuration is actually realized depends on the specific black hole model and must be examined case by case.

In any case, these analyses show that, in the isothermal ensemble, the first law no longer enforces $r_c(r_h)$ to be monotonic, but instead allows nonmonotonic behavior. Once such nonmonotonicity arises, the jump $\Delta_c = r_c(r_{h,l}) - r_c(r_{h,s})$ can be strongly suppressed or even vanish, thereby undermining the reliability of circular orbit radii as encoders of phase transitions. Next, we apply criterion (3.17) to the metric (3.2) to verify the above analysis explicitly.

1. Photon sphere ($\epsilon = 0$)

For the metric (3.2) one obtains

$$\frac{dM}{dr_h} = \frac{1}{(d-1)c_d} \left[2(d-3) r_h^{d-4} + 4(d-2) \pi T_0 r_h^{d-3} - 2(d-2)(d-3) q^2 r_h^{2-d} \right], \quad (3.24)$$

and

$$\Gamma_0 = \frac{2(d-3)}{r_{\text{ps}}} \left[(d-2)q^2 r_{\text{ps}}^{6-2d} - 1 \right]. \quad (3.25)$$

Moreover, $\partial_P \Phi_0 = 0$, and $\partial_M \Phi_0$ agrees with Eq. (3.7).

We now analyze the sign of dM/dr_h . For $q = 0$ one immediately has $dM/dr_h > 0$. For $q \neq 0$, differentiating dM/dr_h gives

$$\begin{aligned} \frac{d^2 M}{dr_h^2} = \frac{1}{(d-1)c_d} & \left[2(d-3)(d-4)r_h^{d-5} \right. \\ & + 4(d-2)(d-3)\pi T_0 r_h^{d-4} \\ & \left. + 2(d-2)^2(d-3)q^2 r_h^{1-d} \right] > 0, \end{aligned} \quad (3.26)$$

so dM/dr_h is strictly increasing in r_h . Meanwhile, From Eq. (3.24),

$$\lim_{r_h \rightarrow 0^+} \frac{dM}{dr_h} = -\infty, \quad \lim_{r_h \rightarrow +\infty} \frac{dM}{dr_h} = +\infty, \quad (3.27)$$

hence there exists a unique r_{h,e_1} such that $dM/dr_h|_{r_{h,e_1}} = 0$. By the criterion (3.18), it follows that:

- $q = 0$: $r_{\text{ps}}(r_h)$ is monotonically increasing;
- $q \neq 0$: $r_{\text{ps}}(r_h)$ is nonmonotonic. It decreases for small r_h , reaches a single minimum at r_{h,e_1} , and then increases.

These results confirm our previous analysis that $r_{\text{ps}}(r_h)$ can indeed become nonmonotonic in the isothermal ensemble, which has not been noticed in earlier studies. Interestingly, in the Sch–AdS case ($q = 0$), $r_{\text{ps}}(r_h)$ remains monotonic. This can be readily understood from Eq. (3.20): When $q = 0$, the slope dP/dr_h is not sufficiently negative to drive dM/dr_h across zero. By contrast, for the RN–AdS case ($q \neq 0$), $P(r_h)$ exhibits a Van der Waals–like behavior, and at small r_h its slope dP/dr_h becomes strongly negative, which is sufficient to make dM/dr_h cross zero.

The explicit expression for dr_{ps}/dr_h reads

$$\begin{aligned} \frac{dr_{\text{ps}}}{dr_h} = & \left[(d-3)(2-d)q^2 r_h^6 \right. \\ & + (d-3+2(d-2)\pi T_0 r_h)r_h^{2d} \left. \right] r_{\text{ps}}^{4+d} / \\ & \left[(d-3)((2-d)q^2 r_{\text{ps}}^6 + r_{\text{ps}}^{2d})r_h^{4+d} \right], \end{aligned} \quad (3.28)$$

For $d = 4$ (the RN–AdS case), this reduces to

$$\frac{dr_{\text{ps}}}{dr_h} = \frac{r_{\text{ps}}^2 \left[2q^2 - r_h^2 (1 + 4\pi T_0 r_h) \right]}{(2q^2 - r_{\text{ps}}^2) r_h^2}, \quad (3.29)$$

and, in the Sch–AdS limit ($q = 0$), further simplifies to

$$\frac{dr_{\text{ps}}}{dr_h} = 1 + 4\pi T_0 r_h. \quad (3.30)$$

This coincides with the standard Sch–AdS result, from which $dr_{\text{ps}}/dr_h > 0$ is immediately evident.

To verify the above analysis, we have performed numerical calculations and displayed the results in Fig. 4. In this figure, T_c denotes the temperature at the RN–AdS critical point, obtained from the criticality conditions $\partial P/\partial r_h = \partial^2 P/\partial r_h^2 = 0$. For the Sch–AdS black hole, $r_{\text{ps}}(r_h)$ begins at $r_{h,\text{min}} = (d-3)/(4\pi T_0)$, where $r_{h,\text{min}}$ is defined by $P(r_{h,\text{min}}) = 0$, and smaller r_h would give $P < 0$ and are therefore discarded as unphysical. It then increases monotonically, remaining globally monotonic in full agreement with Eq. (3.30). In contrast, the RN–AdS black hole exhibits the expected non-monotonic behavior: although $dM/dr_h = 0$ at the extremum, the surface gravity remains positive ($\kappa = 2\pi T_0 > 0$), indicating that the black hole is nonextremal and the curve need not be truncated.

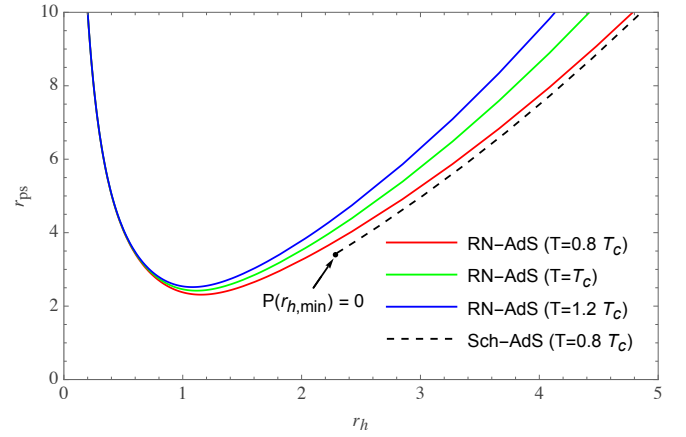


FIG. 4. Behavior of $r_{\text{ps}}(r_h)$ along isothermal paths in $d = 4$. The marked point on the curve corresponds to $P = 0$ at $r_{h,\text{min}} = (d-3)/(4\pi T_0)$, and the unphysical portion with $P < 0$ is truncated. For the Sch–AdS case, we likewise set the temperature to $T = 0.8 T_c$, where T_c is the critical temperature of the RN–AdS solution with $q = 1$. The same choice is adopted for subsequent figures and will not be repeated.

2. ISCO ($\epsilon = 1$)

The metric (3.2) yields

$$\begin{aligned} \frac{dP}{dr_h} = & -\frac{(d-2)}{8\pi} \left[(d-2)(d-3)q^2 r_h^{3-2d} \right. \\ & \left. + (3-d+2\pi T_0 r_h) r_h^{-3} \right], \end{aligned} \quad (3.31)$$

and

$$\begin{aligned} \partial_P \Phi_1 = & \frac{16\pi r_{\text{isco}}}{(d-2)(d-1)} \left[8 + 4(d-1)(d-2)q^2 r_{\text{isco}}^{6-2d} \right. \\ & \left. - c_d(d-1)(d+1)M r_{\text{isco}}^{3-d} \right], \end{aligned} \quad (3.32)$$

where $\partial_P \Phi_1 > 0$ (see Appendix E for proof). Since van der Waals–type behavior occurs only for charged black holes, we analyze the RN–AdS and Sch–AdS cases separately. Moreover, because the explicit expression for dr_c/dr_h is algebraically cumbersome, we focus on whether it changes sign rather than displaying the full formula.

(i) *Sch–AdS* ($q = 0$)

For $q = 0$, Eq. (3.31) reduces to

$$\frac{dP}{dr_h} = -\frac{(d-2)(3-d+2\pi T_0 r_h)}{8\pi r_h^3}. \quad (3.33)$$

It has a single zero at $r_{h,e2} = (d-3)/2\pi T_0$, with $dP/dr_h > 0$ for $r_h < r_{h,e2}$ and $dP/dr_h < 0$ for $r_h > r_{h,e2}$. Using the criterion (3.17), together with $dM/dr_h \partial_M \Phi_1 < 0$, $\Gamma_1 > 0$, and $\partial_P \Phi_1 > 0$, one thus expects $r_{\text{isco}}(r_h)$ to first decrease and then increase. To make this more explicit, we rewrite the criterion (3.17) as

$$\frac{dr_c}{dr_h} = -\frac{1}{\Gamma_\epsilon} \delta(r_{\text{isco}}, r_h, d, q, T_0). \quad (3.34)$$

For sufficiently large r_h one has $dP/dr_h < 0$, which forces $\delta < 0$. It remains to verify that $\delta > 0$ for small r_h , ensuring that δ crosses zero at least once. In this spirit we find

$$\begin{cases} \delta(3r_{h,\min}, r_{h,\min}, 4, 0, T_0) = \frac{1232\pi^2 T_0^2}{27} > 0, & d = 4, \\ \delta(+\infty, r_{h,\min}, d, 0, T_0) = \frac{512\pi^3 T_0^3 r_{\text{isco}}}{(d-3)^2(d-1)} > 0, & d > 4, \end{cases} \quad (3.35)$$

where $r_{h,\min} = (d-3)/(4\pi T_0)$ is defined by $P(r_{h,\min}) = 0$. For $d = 4$ and $P = 0$, the metric (3.2) reduces to the Schwarzschild case, giving $r_{\text{isco}} = 3r_{h,\min}$. For $d > 4$ and $P = 0$, the metric (3.2) reduces to the higher-dimensional Schwarzschild solution, which admits no ISCO. This corresponds to $\lim_{P \rightarrow 0} r_{\text{isco}} = +\infty$, see the end of Appendix E for a brief explanation. Equation (3.35) shows that $\delta > 0$ at small r_h , and together with $\delta < 0$ at sufficiently large r_h this guarantees that δ crosses zero, implying that $r_{\text{isco}}(r_h)$ is necessarily nonmonotonic on its full domain.

(ii) *RN–AdS* ($q \neq 0$)

Since the RN–AdS black hole exhibits a van der Waals–like phase transition, one has

$$\frac{dP}{dr_h} \leq 0 \quad \text{for } T \geq T_c, \quad (3.36)$$

where the equality holds precisely at the critical point $(r_{h,c}, T_c)$. According to the criterion (3.17), when $r_h \geq r_{h,e1}$ (where $r_{h,e1}$ is the zero of dM/dr_h), it follows that $\delta < 0$ and hence $dr_{\text{isco}}/dr_h > 0$, so $r_{\text{isco}}(r_h)$ increases monotonically. For $r_h < r_{h,e1}$, however, δ may become positive. To determine this behavior, we examine the limit $r_h \rightarrow 0^+$.

From Eq. (3.20), one obtains

$$\lim_{r_h \rightarrow 0^+} \frac{dM}{dr_h} = V \frac{dP}{dr_h}, \quad (3.37)$$

which substituted into the criterion (3.17) gives

$$\delta = \frac{dP}{dr_h} (V \partial_M \Phi_1 + \partial_P \Phi_1). \quad (3.38)$$

Meanwhile, from Appendix F, as $r_h \rightarrow 0^+$ one has

$$V \partial_M \Phi_1 \rightarrow -\infty, \quad \partial_P \Phi_1 \rightarrow 0. \quad (3.39)$$

Hence,

$$\delta = \frac{dP}{dr_h} (V \partial_M \Phi_1 + \partial_P \Phi_1) > 0, \quad \Rightarrow \quad \frac{dr_{\text{isco}}}{dr_h} < 0. \quad (3.40)$$

This demonstrates that $r_{\text{isco}}(r_h)$ is nonmonotonic over the full domain of r_h .

The same conclusion holds for $T < T_c$. Along both the small–black hole and large–black hole stable branches, one still has $dP/dr_h < 0$, and the leading-order behavior as $r_h \rightarrow 0^+$ remains identical to the $T \geq T_c$ case above. The only difference is that for $T < T_c$ an intermediate spinodal (unstable) branch appears, on which $dP/dr_h > 0$. Along this segment δ could, in principle, change sign, although this appears unlikely and the branch is dynamically skipped by the first-order phase transition. In any case, viewed globally, $r_{\text{isco}}(r_h)$ is necessarily nonmonotonic for every fixed T_0 . These results again confirm our previous analysis that $r_{\text{isco}}(r_h)$ can indeed exhibit nonmonotonic behavior in the isothermal ensemble.

To verify the above analysis, we perform the numerical check, whose outcome is displayed in Fig. 5. It can be seen that $r_{\text{isco}}(r_h)$ is non-monotonic for both charged and uncharged cases. The distinction lies in that, for the uncharged (Sch–AdS) case, $r_{\text{isco}}(r_h)$ starts at $r_{h,\min} = (d-3)/(4\pi T_0)$, whereas for the charged (RN–AdS) black hole, $P(r_h) > 0$ holds throughout the entire domain.

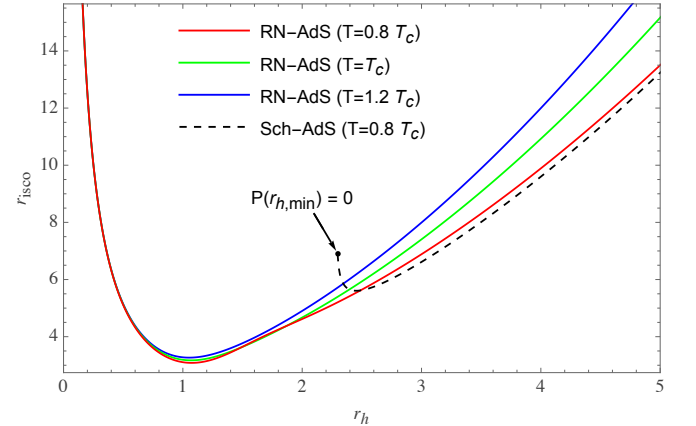


FIG. 5. Behavior of $r_{\text{isco}}(r_h)$ along isothermal paths in $d = 4$.

The breakdown of monotonicity naturally raises two questions. First, as noted above, when $r_c(r_h)$ becomes nonmonotonic, can the jump $\Delta_c = r_c(r_{h,l}) - r_c(r_{h,s})$ across the phase transition be reduced or even vanish? For RN–AdS black holes, the answer is no. In Appendix G, we prove that the extremal radius $r_{h,e}$ of $r_{\text{ps}}(r_h)$ always lies to the left of the small- and large–black hole radii, $r_{h,s}$ and $r_{h,l}$, namely $r_{h,e} < r_{h,s} < r_{h,l}$. So the phase transition always occurs on the increasing branch, indicating that r_{ps} undergoes a jump together with r_h at the phase transition. This behavior is clearly illustrated in Figs. 6 and 7, where the $P(r_c)$ curve preserves the characteristic S-shaped structure of $P(r_h)$. But whether this conclusion holds

for other black holes must be examined case by case. If instead $r_{h,s} < r_{h,e} < r_{h,l}$, the values of $r_{ps}(r_{h,s})$ and $r_{ps}(r_{h,l})$ could become very close or even identical, potentially weakening or even destroying the reliability of using the circular orbit radius to encode the phase transition. It is therefore essential to analyze, from a theoretical perspective, to what extent phase transitions can be encoded in black hole images. This is precisely the role of the general criterion (2.21), which allows one to diagnose the monotonicity of $r_{ps}(r_h)$ in an arbitrary black hole spacetime and thereby assess the reliability of using circular orbit radii to encode phase transitions. Moreover, it is worth noting that, although the proof in Appendix G is presented for the RN–AdS black hole, the underlying method is general and can be applied to other black holes. In particular, we find that the extremal radius of $r_{isco}(r_h)$ always lies below that of $r_{ps}(r_h)$. We expect this ordering to persist in other spacetimes.

Second, can nonmonotonic behavior encode additional thermodynamic information in black hole images? Given that both the black hole shadow and accretion-disk images are closely tied to r_{ps} , we argue that the answer is positive. A simple idea is that the nonmonotonic evolution of black hole images may distinguish isobaric from isothermal ensembles. Further possibilities will be explored in our future work.

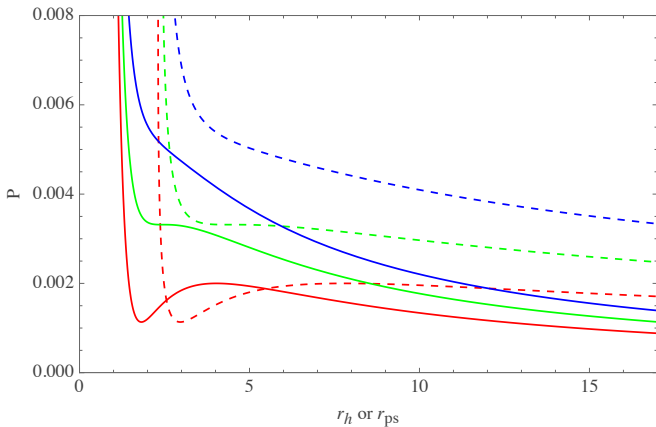


FIG. 6. Isothermal profiles of $P(r_h)$ and $P(r_{ps})$ for $d = 4$ and $q = 1$. The solid and dashed lines correspond to $P(r_h)$ and $P(r_{ps})$, respectively. Both sets of lines are plotted for three temperatures: $T = 0.8T_c$ (red), $T = T_c$ (green), and $T = 1.2T_c$ (blue).

IV. CRITICAL-EXPONENT INVARIANCE

In the previous section, we showed that the mapping $r_c(r_h)$ can exhibit global nonmonotonicity. On the one hand, this implies that encoding phase transitions in the circular orbit radius is not always reliable. On the other hand, from a thermodynamic viewpoint it raises a deeper issue: Whether such global nonmonotonicity can affect the universal critical behavior governed by the neighborhood of the critical point. Specifically, near criticality, the distinction between the coexisting phases becomes progressively weaker and vanishes exactly at the critical point. In conventional thermodynamics, such critical behavior is found to be universal and can be quantitatively

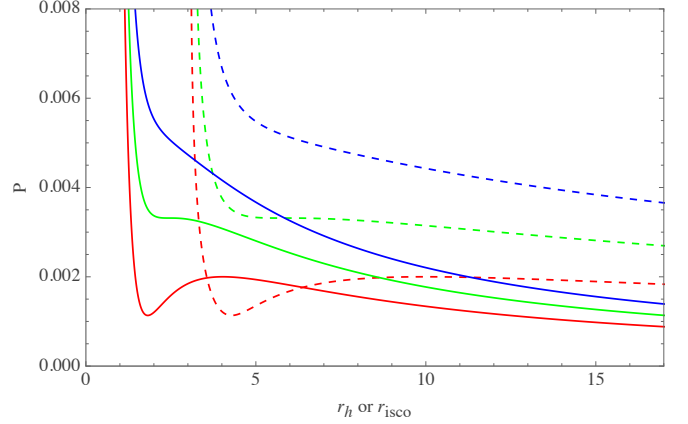


FIG. 7. Isothermal profiles of $P(r_h)$ and $P(r_{isco})$ for $d = 4$ and $q = 1$. The solid and dashed lines correspond to $P(r_h)$ and $P(r_{isco})$, respectively. Both sets of lines are plotted for three temperatures: $T = 0.8T_c$ (red), $T = T_c$ (green), and $T = 1.2T_c$ (blue).

characterized by critical exponents. For example, the classical Van der Waals system exhibits the order-parameter critical exponent $\beta = 1/2$, which has also been shown to hold for many AdS black holes when the thermodynamic volume or the horizon radius is adopted to define the order parameter. Recently, Wei *et al.* demonstrated that in the isobaric ensemble the four-dimensional RN–AdS black hole yields the same value $\beta = 1/2$ when the photon sphere radius is used to define the order parameter, and their numerical results for higher dimensional RN–AdS black holes remain very close to 1/2 [19]. These findings motivate us to test whether such universal critical behavior persists in different ensembles, especially when the mapping $r_c(r_h)$ becomes globally nonmonotonic. In this section we prove that, under both isobaric and isothermal constraints, the mapping $r_c(r_h)$ is necessarily locally monotonic at criticality. As a result, the reparametrization $r_h \mapsto r_c$ reduces to a smooth linear transformation in a neighborhood of the critical point. This guarantees that the critical exponents defined using r_c coincide exactly with those obtained from r_h , so the universal critical behavior is fully preserved.

The order-parameter critical exponent β is defined from the coexistence gap of the horizon radius for $T < T_c$:

$$\Delta r_h := r_{h,l} - r_{h,s} \sim |t|^\beta, \quad t := \frac{T - T_c}{T_c} \rightarrow 0^-, \quad (4.1)$$

We will show that the circular orbit radius inherits the same scaling, namely

$$\Delta r_c := r_c(r_{h,l}) - r_c(r_{h,s}) \sim |t|^\beta. \quad (4.2)$$

The proof of Eq. (4.2) is straightforward. We first show that $r_c(r_h)$ is monotonic in the neighborhood of the critical point and then demonstrate that such a monotonic reparametrization leaves the critical exponents unchanged. Near the critical point one has $dP/dr_h \rightarrow 0$, so that the isothermal criterion (3.17) reduces to

$$\frac{dr_c}{dr_h} = -\frac{1}{\Gamma_\epsilon} \frac{dM}{dr_h} \partial_M \Phi_\epsilon, \quad (4.3)$$

which coincides exactly with the isobaric criterion (3.6). Consequently, in both ensembles the monotonic behavior of $r_c(r_h)$ near the critical point is entirely determined by that of $M(r_h)$. In the isobaric ensemble, the first law enforces $dM/dr_h > 0$, and $r_c(r_h)$ remains monotonic. In the isothermal ensemble, the first law gives

$$\frac{dM}{dr_h} = T_0 S'(r_h) + V \frac{dP}{dr_h}, \quad (4.4)$$

which simplifies near the critical point to

$$\frac{dM}{dr_h} = T_0 S'(r_h), \quad (4.5)$$

again ensuring $dM/dr_h > 0$ and hence the monotonicity of $r_c(r_h)$. Therefore, in both the isobaric and isothermal ensembles,

$$C := \left. \frac{dr_c}{dr_h} \right|_c \neq 0. \quad (4.6)$$

We next expand $r_c(r_h)$ about the critical radius $r_{h,c}$ as

$$r_c(r_h) = r_{c,c} + C(r_h - r_{h,c}) + o(|r_h - r_{h,c}|). \quad (4.7)$$

This immediately yields

$$\Delta r_c = r_{c,l} - r_{c,s} = C \Delta r_h + o(\Delta r_h) \sim |t|^\beta, \quad (4.8)$$

which shows that, provided $C \neq 0$, the leading behavior of Δr_c near the critical point is governed by Δr_h . As a result, the critical exponent remains unchanged:

$$\beta_{(r_c)} = \beta_{(r_h)}. \quad (4.9)$$

This result is noteworthy: Although $r_c(r_h)$ may exhibit global nonmonotonic behavior, it must be monotonic in the neighborhood of the critical point, which ensures that the critical exponent remains invariant under reparametrization. This shows that the circular orbit radius encodes not only the existence of phase transitions but also their universal critical properties. Moreover, it is worth emphasizing that this proof does not rely on the specific form of the metric (3.2), but only on the criterion (3.17) and the first law. The result therefore applies, in principle, to any black hole with $\partial_M \Phi_\epsilon \neq 0$, which points to a more fundamental connection between black hole gravitational geometry and thermodynamics.

V. SUMMARY AND DISCUSSION

In this paper, we derived the monotonicity criterion (2.21) that applies to arbitrary thermodynamic paths in the parameter space of any static, spherically symmetric black hole, thereby clarifying when the mapping between the horizon radius r_h and the circular orbit radius r_c is monotonic. In this framework, the monotonicity of $r_c(r_h)$ is governed by two factors: (i) the intrinsic geometric/orbital properties of the black hole and (ii) the chosen path in the extended thermodynamic parameter space. For any nonextremal black hole admitting an

unstable photon sphere or an ISCO, the first factor does not by itself induce nonmonotonicity, whereas the second is decisive. Motivated by this, we take the d -dimensional RN–AdS black hole as a concrete example and analyze two thermodynamically cases: the isobaric and isothermal ensembles.

Our results show that the monotonicity of $r_c(r_h)$ is completely different in the two ensembles, and this contrast is closely tied to the first law of black hole thermodynamics. In the isobaric ensemble, the sign of dr_c/dr_h is determined by $\partial_M \Phi_\epsilon$ together with dM/dr_h . For RN–AdS, $\partial_M \Phi_\epsilon \neq 0$, while the first law enforces $dM/dr_h > 0$, so dr_c/dr_h does not change sign and $r_c(r_h)$ is globally monotonic (both $r_{ps}(r_h)$ and $r_{isco}(r_h)$ are strictly increasing). This monotonic increase guarantees that, whenever a phase transition occurs, r_c jumps together with r_h , thereby ensuring that the circular orbit radius reliably encodes the phase transition information. By the universality of the first law, this conclusion is not restricted to RN–AdS but extends to any black hole with $\partial_M \Phi_\epsilon \neq 0$.

In contrast, in the isothermal ensemble the sign of dr_c/dr_h is controlled by four factors: $\partial_M \Phi_\epsilon$, $\partial_P \Phi_\epsilon$, dM/dr_h , and dP/dr_h . For the photon sphere one has $\partial_P \Phi_0 = 0$, so the sign of dr_{ps}/dr_h again depends only on $\partial_M \Phi_0$ and dM/dr_h , but now the first law allows dM/dr_h to cross zero. As a result, dr_{ps}/dr_h may change sign and $r_{ps}(r_h)$ can become nonmonotonic. This is precisely what happens for the RN–AdS black hole, whose $r_{ps}(r_h)$ indeed exhibits nonmonotonic behavior, whereas the Sch–AdS case is exceptional: The absence of charge eliminates any zero of dM/dr_h , so $r_{ps}(r_h)$ remains monotonic. For the ISCO, one has $\partial_P \Phi_1 > 0$, so the sign of dr_{isco}/dr_h is jointly controlled by dM/dr_h and dP/dr_h . The first law forces these two derivatives to share the same sign in certain ranges of r_h , thereby making sign changes in dr_{isco}/dr_h possible. This possibility is realized explicitly in RN–AdS and Sch–AdS, where $r_{isco}(r_h)$ is fully nonmonotonic. Given the universality of the first law, we expect similar nonmonotonic behavior to appear for other black holes evolving along isotherms. In principle, such nonmonotonicity could reduce the jump in r_c at the phase transition, or even eliminate it, thereby undermining the reliability of using r_c to encode the phase transition.

Fortunately, we have shown that, for RN–AdS, the phase transition always takes place on an increasing branch of $r_c(r_h)$, so the reliability of using r_c to encode the phase transition is not compromised. Whether this remains true for other black holes requires further case-by-case checks: One must first establish whether $r_c(r_h)$ becomes nonmonotonic in the isothermal ensemble and then determine whether this nonmonotonicity alters the jump amplitude $\Delta r_c = r_{c,l} - r_{c,s}$ across the phase transition. Both steps rest on the monotonicity criterion (2.21), so in this sense our work provides an effective theoretical framework for assessing the observability of black hole phase transitions.

It is also worth emphasizing that the nonmonotonic behavior of $r_c(r_h)$ in the isothermal ensemble has, to our knowledge, gone unnoticed so far. Thus, previous studies have largely focused on extracting phase transition information from black hole optical appearances, whereas we now identify an additional channel: The nonmonotonic evolution of the optical appearance can provide a diagnostic of the underlying ther-

mododynamic ensemble. Since any nonmonotonicity of $r_c(r_h)$ should be reflected in the black hole image, such a test is feasible in principle. Of course, from an observational perspective, the relevant observables are the shadow and the accretion-disk image rather than r_{ps} or r_{isco} directly. Thus our next step is to analyze how the shadow and accretion-disk images evolve under isobaric versus isothermal processes.

Finally, we prove that whenever a black hole exhibits critical behavior, the first law alone guarantees invariance of the critical exponents under the reparametrization $r_h \rightarrow r_c$ for any spacetime satisfying $\partial_M \Phi_\epsilon \neq 0$. This shows that circular particle orbits not only encode phase transitions but also retain the universal critical behavior of black hole thermodynamics. This generality hints at a deeper geometric-thermodynamic correspondence that merits further study.

ACKNOWLEDGMENTS

We would like to thank Zhongzhinan Dong and Jiawei Chen for helpful discussions. This work is supported in part by NSFC Grants No. 12165005 and No. 11961131013.

Appendix A: Preservation of Functional Behavior under Monotonic Reparameterization

Suppose that $F(x)$ is a differentiable function defined on an interval $I \subset \mathbb{R}$, and let x_m denote its m -th zero, so that $F(x_m) = 0$. Now introduce a new variable y and assume a smooth, strictly monotonic mapping

$$x = x(y), \quad y \in J \subset \mathbb{R}, \quad (\text{A1})$$

with $dx/dy \neq 0$ for all $y \in J$. We then reparameterize $F(x)$ as

$$\tilde{F}(y) = F(x(y)). \quad (\text{A2})$$

Applying the chain rule gives

$$\frac{d\tilde{F}}{dy} = \frac{dF}{dx} \frac{dx}{dy}. \quad (\text{A3})$$

Since $dx/dy \neq 0$, one immediately has

$$\frac{d\tilde{F}}{dy} = 0 \iff \frac{dF}{dx} = 0. \quad (\text{A4})$$

Thus, the stationary points of F and \tilde{F} correspond one-to-one: each stationary point x_m of F maps to a stationary point $y_m = x^{-1}(x_m)$ of \tilde{F} , and vice versa.

To demonstrate that the nature of the stationary points is preserved, we differentiate once more:

$$\frac{d^2\tilde{F}}{dy^2} = \frac{d^2F}{dx^2} \left(\frac{dx}{dy} \right)^2 + \frac{dF}{dx} \frac{d^2x}{dy^2}. \quad (\text{A5})$$

At a stationary point y_m where $dF/dx = 0$, this reduces to

$$\frac{d^2\tilde{F}}{dy^2} \bigg|_{y_m} = \frac{d^2F}{dx^2} \bigg|_{x_m} \left(\frac{dx}{dy} \right)^2 \bigg|_{y_m}. \quad (\text{A6})$$

Since $(dx/dy)^2 > 0$, it follows that

$$\begin{aligned} \frac{d^2F}{dx^2} \bigg|_{x_m} > 0 &\implies \frac{d^2\tilde{F}}{dy^2} \bigg|_{y_m} > 0, \\ \frac{d^2F}{dx^2} \bigg|_{x_m} < 0 &\implies \frac{d^2\tilde{F}}{dy^2} \bigg|_{y_m} < 0. \end{aligned} \quad (\text{A7})$$

Hence, under any smooth and monotonic reparameterization $x \mapsto y$, a local minimum (maximum) of F remains a local minimum (maximum) of \tilde{F} .

Away from the stationary points, Eq. (A3) implies that when $dx/dy > 0$, the signs of $d\tilde{F}/dy$ and dF/dx coincide, whereas for $dx/dy < 0$ they are opposite. Geometrically, the former corresponds to a horizontal stretching of the original curve, while the latter involves both stretching and a reflection about the x -axis. In either case, the overall qualitative profile of the function remains unchanged.

If F is identified with the thermodynamic temperature T or pressure P of a black hole, and the variables are smoothly and monotonically related as $x = r_h$ and $y = r_c$, then under the mapping $r_h \mapsto r_c$ the functions $T(r_c)$ and $P(r_c)$ retain their characteristic van der Waals-like S -shaped structure. As a result, during the small-to-large black hole phase transition, the critical radius r_c undergoes a finite discontinuous jump.

Appendix B: Constructive counterexample in Sch–AdS demonstrating that $r_{\text{ps}}(r_h)$ can decrease

For the four-dimensional Sch–AdS black hole, the metric function reads

$$f(r) = 1 - \frac{2M}{r} + \frac{8\pi P}{3} r^2, \quad (\text{B1})$$

where M is the ADM mass and $P = -\Lambda/(8\pi)$ denotes the thermodynamic pressure. The photon sphere condition $rf'(r) - 2f(r) = 0$ gives

$$r_{\text{ps}} = 3M, \quad (\text{B2})$$

indicating that r_{ps} is independent of P . The event horizon radius r_h satisfies $f(r_h; M, P) = 0$, from which we obtain

$$M = \frac{r_h}{2} + \frac{4\pi P}{3} r_h^3. \quad (\text{B3})$$

Eliminating M between Eqs. (B2) and (B3) yields

$$r_{\text{ps}}(r_h) = \frac{3r_h}{2} + 4\pi P r_h^3. \quad (\text{B4})$$

Figure 8 illustrates $r_{\text{ps}}(r_h)$ for nine representative values of P , without imposing any specific relation between P and M .

Next, we impose the path constraint

$$P(M) = -\frac{3k^2(b + (-1 + 2k)M)}{8\pi(b - M)^3}, \quad (\text{B5})$$

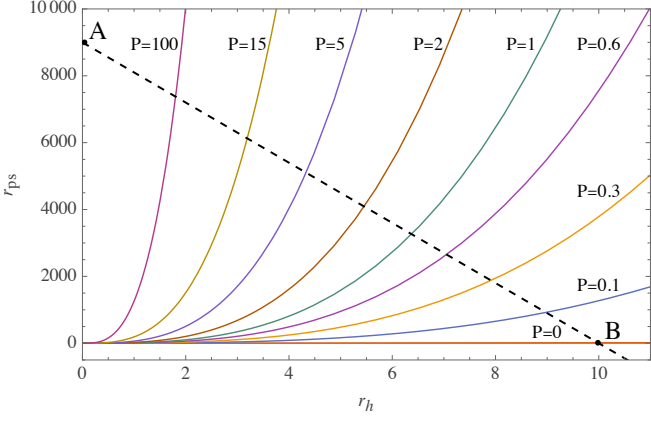


FIG. 8. Plots of $r_{\text{ps}}(r_h)$ for the Sch–AdS black hole. Colored solid curves denote nine different pressures P , and the black dashed curve shows the path-constrained case with $k < 0$ and $b > 0$.

where k is a dimensionless constant and b carries dimensions of mass. Substituting Eqs. (B5), (B3), and (B2) gives a simple linear relation,

$$r_{\text{ps}}(r_h) = 3(k r_h + b). \quad (\text{B6})$$

In Fig. 8, this corresponds to the black dashed line, which decreases monotonically between points A and B . Its intersections with the colored curves are uniquely determined by the constraint (B5). Along this dashed segment, all physical requirements are satisfied: $M > 0$, $r_h > 0$, $P > 0$, and the surface gravity remains strictly positive,

$$\kappa = \frac{1}{2} \partial_r f(r)|_{r_h} = \frac{M}{r_h^2} + \frac{8\pi P r_h}{3} > 0, \quad (\text{B7})$$

ensuring non-extremality.

This simple example illustrates that the monotonicity of $r_{\text{ps}}(r_h)$ [and likewise of $r_{\text{isco}}(r_h)$] is governed not only by the functional dependence of (M, P) in $f(r)$, but also by the parameter path that links M and P . Appropriate constraints can thus lead to a non-increasing behavior of $r_{\text{ps}}(r_h)$. Applying the criterion (2.21) yields

$$\frac{dr_{\text{ps}}}{dr_h} = \frac{2\kappa}{\Gamma_0} \frac{\partial_M \Phi_0}{\partial_M f + \partial_P f \frac{dP}{dM}}, \quad (\text{B8})$$

where

$$\frac{dP}{dM} = -\frac{3k^2(b + bk + 2kM - M)}{4\pi(b - M)^4}. \quad (\text{B9})$$

After straightforward algebra, we obtain

$$\frac{dr_{\text{ps}}}{dr_h} = 3k, \quad (\text{B10})$$

which agrees with Eq. (B6).

Appendix C: Conditions of the photon sphere and ISCO

For photons ($\epsilon = 0$) the radial function (2.5) reduces to

$$\mathcal{R}(r) = E^2 - \frac{f(r) L^2}{r^2}. \quad (\text{C1})$$

Imposing the circular-orbit condition, $\mathcal{R}'(r_c) = 0$, gives

$$\mathcal{R}'(r_{\text{ps}}) = -\frac{f'(r_{\text{ps}}) L^2}{r_{\text{ps}}^3} + \frac{2f(r_{\text{ps}}) L^2}{r_{\text{ps}}^3} = 0. \quad (\text{C2})$$

Eliminating L^2 yields

$$\Phi_0(r_{\text{ps}}) := r_{\text{ps}} f'(r_{\text{ps}}) - 2f(r_{\text{ps}}) = 0, \quad (\text{C3})$$

which corresponds to the photon-sphere equation (2.7). Imposing the instability of the photon circular orbit, $\mathcal{R}''(r_{\text{ps}}) > 0$, gives

$$\mathcal{R}''(r_{\text{ps}}) = -\frac{L^2}{r_{\text{ps}}^3} \underbrace{[r_{\text{ps}} f''(r_{\text{ps}}) - f'(r_{\text{ps}})]}_{\equiv \partial_r \Phi_0(r_{\text{ps}})} > 0. \quad (\text{C4})$$

Since $L^2/r_{\text{ps}}^3 > 0$, it follows that

$$\Gamma_0 := \partial_r \Phi_0(r_{\text{ps}}) = r_{\text{ps}} f''(r_{\text{ps}}) - f'(r_{\text{ps}}) < 0, \quad (\text{C5})$$

which corresponds to the stability criterion (2.9).

For massive particles ($\epsilon = 1$) the radial function (2.5) reduces to

$$\mathcal{R}(r) = E^2 - f(r) \left(1 + \frac{L^2}{r^2}\right). \quad (\text{C6})$$

The conditions

$$\mathcal{R}'(r_{\text{isco}}) = \mathcal{R}''(r_{\text{isco}}) = 0, \quad (\text{C7})$$

give two algebraic equations for L and r_{isco} :

$$\mathcal{R}'(r_{\text{isco}}) = \frac{2f(r_{\text{isco}}) L^2}{r_{\text{isco}}^3} - f'(r_{\text{isco}}) \left(1 + \frac{L^2}{r_{\text{isco}}^2}\right) = 0, \quad (\text{C8})$$

$$\begin{aligned} \mathcal{R}''(r_{\text{isco}}) = & -\frac{6f(r_{\text{isco}}) L^2}{r_{\text{isco}}^4} + \frac{4f'(r_{\text{isco}}) L^2}{r_{\text{isco}}^3} \\ & - f''(r_{\text{isco}}) \left(1 + \frac{L^2}{r_{\text{isco}}^2}\right) = 0. \end{aligned} \quad (\text{C9})$$

Eliminating L^2 yields

$$\mathcal{R}''(r_{\text{isco}}) = \frac{2\Phi_1(r_{\text{isco}})}{r_{\text{isco}}^2 f'(r_{\text{isco}}) - 2r_{\text{isco}} f(r_{\text{isco}})} = 0, \quad (\text{C10})$$

where we define

$$\begin{aligned} \Phi_1(r_{\text{isco}}) := & r_{\text{isco}} f(r_{\text{isco}}) f''(r_{\text{isco}}) - 2r_{\text{isco}} [f'(r_{\text{isco}})]^2 \\ & + 3f(r_{\text{isco}}) f'(r_{\text{isco}}) = 0 \end{aligned} \quad (\text{C11})$$

which corresponds to the ISCO equation (2.11). To determine the sign of

$$\Gamma_1 := \partial_r \Phi_1(r_{\text{isco}}), \quad (\text{C12})$$

we rewrite Eq. (C10) as

$$\mathcal{R}''(r_c) = \frac{2 \Phi_1(r_c)}{r_c^2 f'(r_c) - 2r_c f(r_c)}, \quad (\text{C13})$$

where r_c denotes the radius of a timelike circular orbit in the neighborhood of the ISCO. By definition of the ISCO, orbits with $r_c > r_{\text{isco}}$ are stable ($\mathcal{R}''(r_c) < 0$), whereas those with $r_c < r_{\text{isco}}$ are unstable ($\mathcal{R}''(r_c) > 0$). Next, We analyze the sign of $\mathcal{R}''(r_c)$, which is fixed by the numerator and denominator of the ratio above. We abbreviate the denominator as

$$D(r_c) := r_c^2 f'(r_c) - 2r_c f(r_c) = r_c^4 \partial_r \left(\frac{f}{r^2} \right) \Big|_{r_c}, \quad (\text{C14})$$

where $V(r) \propto f(r)/r^2$ is the photon effective potential. For $r > r_{\text{ps}}$ one has $\partial_r V < 0$, and circular orbits near the ISCO satisfy $r_c > r_{\text{ps}}$. Therefore $D(r_c) < 0$. We now examine the numerator. Expanding Φ_1 about the ISCO,

$$\Phi_1(r_c) = \Phi_1(r_{\text{isco}}) + \partial_r \Phi_1(r_{\text{isco}}) (r_c - r_{\text{isco}}) + O[(r_c - r_{\text{isco}})^2], \quad (\text{C15})$$

and using $\Phi_1(r_{\text{isco}}) = 0$, we obtain near r_{isco} :

$$\text{sgn} [\mathcal{R}''(r_c)] = \text{sgn} \left[\frac{\partial_r \Phi_1(r_{\text{isco}}) (r_c - r_{\text{isco}})}{D(r_{\text{isco}})} \right]. \quad (\text{C16})$$

Consequently, to ensure $\mathcal{R}''(r_c) > 0$ for $r_c < r_{\text{isco}}$ and $\mathcal{R}''(r_c) < 0$ for $r_c > r_{\text{isco}}$, the slope of Φ_1 at the ISCO must be positive, $\Gamma_1 := \partial_r \Phi_1(r_{\text{isco}}) > 0$, which is precisely the stability criterion (2.12).

Appendix D: Local Existence of $M(r_h)$ and $P(r_h)$

Consider the two constraint equations at the horizon,

$$f(r_h; M, P) = 0, \quad T(r_h; M, P) = T_0, \quad (\text{D1})$$

where both f and T are assumed to be smooth in (M, P) . Differentiating these relations and treating r_h as the path parameter gives

$$\begin{aligned} \partial_{r_h} f \, dr_h + \partial_M f \, dM + \partial_P f \, dP &= 0, \\ \partial_{r_h} T \, dr_h + \partial_M T \, dM + \partial_P T \, dP &= 0. \end{aligned} \quad (\text{D2})$$

Eliminating dP and dM in turn yields

$$\begin{aligned} \frac{dM}{dr_h} &= - \frac{\partial_{r_h} f \, \partial_P T - \partial_P f \, \partial_{r_h} T}{\partial_M f \, \partial_P T - \partial_P f \, \partial_M T}, \\ \frac{dP}{dr_h} &= - \frac{\partial_{r_h} f \, \partial_M T - \partial_M f \, \partial_{r_h} T}{\partial_M f \, \partial_P T - \partial_P f \, \partial_M T}. \end{aligned} \quad (\text{D3})$$

Defining

$$\Delta := \partial_M f \, \partial_P T - \partial_P f \, \partial_M T, \quad (\text{D4})$$

we see that the nondegeneracy condition $\Delta \neq 0$ guarantees—by the implicit function theorem—the local existence and uniqueness of smooth functions $M(r_h)$ and $P(r_h)$ satisfying the two constraints in a neighborhood of a reference point. When $\Delta = 0$, this parametrization in terms of r_h breaks down and the curve must be reparametrized. For the metric (3.2), one finds

$$\Delta = - \frac{4c_d}{d-2} r_h^{4-d} \neq 0. \quad (\text{D5})$$

Appendix E: Proof of the Positivity of $\partial_P \Phi_1$

$$\begin{aligned} \partial_P \Phi_1 &= \frac{16\pi r_{\text{isco}}}{(d-2)(d-1)} \left[8 + 4(d-1)(d-2)q^2 r_{\text{isco}}^{6-2d} \right. \\ &\quad \left. - c_d(d-1)(d+1)M r_{\text{isco}}^{3-d} \right]. \end{aligned} \quad (\text{E1})$$

Since the prefactor is positive, the sign of $\partial_P \Phi_1$ is determined by the bracketed term. Let $x := r_{\text{isco}}^{d-3} > 0$, so that

$$B = 8 + \frac{4(d-1)(d-2)q^2}{x^2} - \frac{(d-1)(d+1)c_d M}{x}. \quad (\text{E2})$$

Multiplying both sides by $x^2 > 0$ yields an upward-opening quadratic,

$$Q(x) = 8x^2 - (d-1)(d+1)c_d M x + 4(d-1)(d-2)q^2, \quad (\text{E3})$$

with discriminant

$$\Delta_x = [(d-1)(d+1)c_d M]^2 - 128(d-1)(d-2)q^2, \quad (\text{E4})$$

and roots

$$x_{\pm} = \frac{(d-1)(d+1)c_d M \pm \sqrt{\Delta_x}}{16}, \quad (\Delta_x \geq 0). \quad (\text{E5})$$

Hence,

$$\text{sgn} (\partial_P \Phi_1) = \begin{cases} +, & \Delta_x < 0 \text{ or } x \in (0, x_-) \cup (x_+, +\infty), \\ 0, & x = x_{\pm}, \\ -, & x \in (x_-, x_+). \end{cases} \quad (\text{E6})$$

To determine the sign of $\partial_P \Phi_1$, we first examine the sign of Δ_x . Under the isothermal constraint one has

$$T_0 = \frac{(d-1)c_d M r_h^{d+3} - 2(d-2)q^2 r_h^6 - 2r_h^{2d}}{4\pi r_h^{1+2d}}. \quad (\text{E7})$$

The requirement $T_0 > 0$ is equivalent to

$$(d-1)c_d M r_h^{d+3} - 2(d-2)q^2 r_h^6 - 2r_h^{2d} > 0. \quad (\text{E8})$$

Introducing $r_h^{2d} = r_h^6 s^2$ and $r_h^{d+3} = r_h^6 s$, we define

$$\mathcal{B}(s) := -2s^2 + (d-1)c_d M s - 2(d-2)q^2 > 0, \quad (\text{E9})$$

which is a downward-opening quadratic function. For $\mathcal{B}(s) > 0$ to hold, its discriminant must satisfy

$$\Delta_s = (c_d(d-1)M)^2 - 16(d-2)q^2 > 0, \quad (\text{E10})$$

implying

$$M > \frac{4\sqrt{d-2}}{c_d(d-1)} q. \quad (\text{E11})$$

Substituting this inequality into Eq. (E4) gives

$$\Delta_x > 0. \quad (\text{E12})$$

Hence, $\partial_P \Phi_1$ may take positive, negative, or zero values, depending on the relative magnitude of x and x_{\pm} .

To clarify the relation between x and x_{\pm} , we rewrite

$$\Phi_1(r, M, q, P, d) = P \partial_P \Phi_1 + \tilde{\Phi}_1(r, M, q, d). \quad (\text{E13})$$

Fixing M , q , and d at finite values and taking the limit $P \rightarrow +\infty$, the condition $\Phi_1(r, M, q, P, d) = 0$ can be satisfied only if

$$\partial_P \Phi_1 \rightarrow 0. \quad (\text{E14})$$

This shows that the quantities $x_{\pm}^{1/(d-3)}$ correspond exactly to the limiting values of r_{isco} as $P \rightarrow +\infty$. Next, we examine the limit $P \rightarrow 0$. For $d = 4$, one obtains

$$\Phi_1 = \frac{2Mr_{\text{isco}}^2(r_{\text{isco}} - 6M) + 18Mq^2r_{\text{isco}} - 8q^4}{r_{\text{isco}}^5}. \quad (\text{E15})$$

The analysis can be divided into two cases:

- $q = 0$: For the Schwarzschild black hole, this yields $r_{\text{isco}} = 6M$. In this case, the two roots are $x_{\pm} = 15M/4$ and 0, and clearly $x|_{P=0} = 6M > x_{+}$.
- $q \neq 0$: For the RN black hole, it is well known that r_{isco} attains its minimum at $M = q$, where $r_{\text{isco,min}} = 4M$. From Eq. (E5), x_{+} decreases monotonically with q , reaching its maximum $x_{+,\text{max}} = 15M/4$ at $q = 0$, so that $x_{\min}|_{P=0} = 4M > x_{+,\text{max}} = 15M/4$.

Therefore, for both the Schwarzschild and RN black holes one always has $x|_{P=0} > x_{+}$, and consequently $\partial_P \Phi_1 > 0$ in this limit.

Next, consider increasing P from zero in Eq. (E13). Initially, one has $\Phi_1 = \tilde{\Phi}_1(r_{\text{isco}}|_{P=0}, M, q, d) = 0$ with $\Gamma_1 = \partial_r \tilde{\Phi}_1 > 0$. Once P increases, the term $\partial_P \Phi_1 > 0$ appears, so $\tilde{\Phi}_1$ must decrease to maintain $\Phi_1 = 0$. Since $\Gamma_1 > 0$, this requires r_{isco} to decrease, meaning that x moves toward x_{+} . As P continues to increase, we assume continuous dependence of r_{isco} and $\partial_P \Phi_1$ on P , so that x must vary continuously from $x|_{P=0}$ to $x_{+}|_{P \rightarrow +\infty}$.

Consequently, for any finite P , the corresponding x must lie within the interval $(x_{+}, x|_{P=0})$, which guarantees $\partial_P \Phi_1 > 0$ throughout. From a physical viewpoint, this reflects the suppressive effect of pressure on the ISCO radius: as P increases, r_{isco} decreases monotonically toward x_{+} .

For higher dimensions ($d > 4$), the argument becomes even simpler. At $P = 0$, Schwarzschild and RN black holes possess no ISCO ($r_{\text{isco}} \rightarrow +\infty$). As P increases, r_{isco} moves inward from infinity toward x_{+} , again ensuring $\partial_P \Phi_1 > 0$. Hence, in all cases we conclude that

$$\partial_P \Phi_1 > 0. \quad (\text{E16})$$

The limit used above,

$$\lim_{P \rightarrow 0} r_{\text{isco}} = +\infty, \quad (\text{E17})$$

can be argued as follows. For the higher-dimensional Schwarzschild black hole ($q = 0, d > 4$), the ISCO condition takes the form

$$\begin{aligned} \Phi_1(r_{\text{isco}}) = & \frac{16\pi P r_{\text{isco}}}{(d-2)(d-1)} \left[8 - c_d(d^2-1)M r_{\text{isco}}^{3-d} \right. \\ & - c_d(d-3)M r_{\text{isco}}^{2(1-d)} \left[c_d(d-1)M r_{\text{isco}}^3 \right. \\ & \left. \left. + (d-5) r_{\text{isco}}^d \right] \right]. \end{aligned} \quad (\text{E18})$$

If r_{isco} remains finite as $P \rightarrow 0$, the first (pressure-dependent) term vanishes and Φ_1 reduces to

$$\begin{aligned} \Phi_1(r_{\text{isco}}) = & -c_d(d-3)M r_{\text{isco}}^{2(1-d)} \left[c_d(d-1)M r_{\text{isco}}^3 \right. \\ & \left. + (d-5) r_{\text{isco}}^d \right], \end{aligned} \quad (\text{E19})$$

which admits no positive root for r_{isco} when $d > 4$. Thus a finite r_{isco} is incompatible with the ISCO condition in this limit. By contrast, if $r_{\text{isco}} \rightarrow +\infty$ as $P \rightarrow 0$, the second term in Φ_1 is suppressed, and one finds

$$\Phi_1(r_{\text{isco}}) \simeq \frac{128\pi P r_{\text{isco}}}{(d-2)(d-1)}, \quad (\text{E20})$$

so that the product $P r_{\text{isco}}$ can tend to zero as $P \rightarrow 0$. Therefore the ISCO condition can be satisfied only if

$$\lim_{P \rightarrow 0} r_{\text{isco}} = +\infty. \quad (\text{E21})$$

For the higher-dimensional RN black hole ($q \neq 0, d > 4$), the ISCO condition takes the form

$$\begin{aligned} \Phi_1(r_{\text{isco}}) = & -2(d-3)q r_{\text{isco}}^{2(1-2d)} (-q r_{\text{isco}}^3 + r_{\text{isco}}^d)^2 \\ & \times [2(d-2)q r_{\text{isco}}^3 + (d-5)r_{\text{isco}}^d] \\ & + \frac{32\pi P r_{\text{isco}}}{(d-2)(d-1)} \left\{ 4 - (d-1)q r_{\text{isco}}^{3-2d} \right. \\ & \left. \times [-2(d-2)q r_{\text{isco}}^3 + (d+1)r_{\text{isco}}^d] \right\}, \end{aligned} \quad (\text{E22})$$

where we have imposed the extremality condition $M = 2q/c_d$. Repeating the same analysis as in the Schwarzschild case then yields Eq. (E17).

Appendix F: Asymptotic Relations in the Small-Horizon Limit

We now examine the asymptotic behavior of $V \partial_M \Phi_1$ and $\partial_P \Phi_1$ in the small-horizon limit ($r_h \rightarrow 0^+$), focusing on their leading divergent terms.

For $\partial_P \Phi_1$, since $r_h \rightarrow 0^+$ implies $P \rightarrow +\infty$, one has $\partial_P \Phi_1 \rightarrow 0$ (see Appendix E for details). The thermodynamic volume takes the simple form

$$V = \frac{\Omega_{d-2} r_h^{d-1}}{d-1}, \quad (\text{F1})$$

and therefore vanishes as $V \sim r_h^{d-1} \rightarrow 0$. $\partial_M \Phi_1$ reads

$$\begin{aligned} \partial_M \Phi_1 = & 3c_d(d-1)(d-3)q^2 r_{\text{isco}}^{8-3d} \\ & - 2c_d^2(d-1)(d-3)M r_{\text{isco}}^{5-2d} \\ & - c_d(d-3)(d-5)r_{\text{isco}}^{2-d} \\ & - \frac{16c_d(d+1)\pi P r_{\text{isco}}^{4-d}}{d-2}, \end{aligned} \quad (\text{F2})$$

and its asymptotic behavior can be inferred once the leading scalings of M , P , and r_{isco} are determined.

Under the isothermal constraint, one finds

$$M(r_h) = \frac{(1+2\pi T_0 r_h) r_h^{2(d-3)} + 2(d-2)q^2}{c_d(d-1)r_h^{d-3}}, \quad (\text{F3})$$

and

$$P(r_h) = \frac{(d-2)[(3-d+4\pi T_0 r_h) r_h^{2(d-3)} + (d-3)q^2]}{16\pi r_h^{2(d-2)}}. \quad (\text{F4})$$

In the small-horizon limit ($r_h \rightarrow 0^+$), these behave as

$$M \sim \frac{1}{r_h^{d-3}}, \quad P \sim \frac{1}{r_h^{2(d-2)}}. \quad (\text{F5})$$

For the ISCO, the divergence $P \rightarrow +\infty$ implies (see Appendix E)

$$r_{\text{isco}}^{d-3} \rightarrow x_+ = \frac{(d-1)(d+1)c_d M + \sqrt{\Delta_x}}{16}, \quad (\text{F6})$$

where

$$\Delta_x = [(d-1)(d+1)c_d M]^2 - 128(d-1)(d-2)q^2. \quad (\text{F7})$$

Near $r_h \rightarrow 0^+$, the dominant contribution arises from the mass term M , so that

$$r_{\text{isco}} \sim M^{\frac{1}{d-3}} \sim \frac{1}{r_h}. \quad (\text{F8})$$

Substituting Eqs. (F5) and (F8) into Eq. (F2) gives $\partial_M \Phi_1 \sim -r_h^{-d}$, and hence

$$V \partial_M \Phi_1 \sim -\frac{1}{r_h} \rightarrow -\infty. \quad (\text{F9})$$

Appendix G: Monotonicity of $r_c(r_h)$ in the Phase Transition Region

We take the four-dimensional case as an example and show that the phase transition occurs only along the increasing

branch of $r_c(r_h)$. The proof strategy is simple: we numerically scan the parameter space, extract the extremal radius $r_{h,e}$ of $r_{\text{ps}}(r_h)$ and the small-black hole radius $r_{h,s}$ at phase coexistence, and then compare their values. In the isothermal ensemble the free parameters are the temperature T_0 and the charge q . Conveniently, the explicit q -dependence can be removed by introducing reduced (dimensionless) variables

$$\tilde{r}_h = \frac{r_h}{r_{h,c}}, \quad \tilde{M} = \frac{M}{M_c}, \quad \tilde{P} = \frac{P}{P_c}, \quad \tilde{T} = \frac{T}{T_c}, \quad (\text{G1})$$

where the critical values at the thermodynamic critical point are

$$\begin{aligned} r_{h,c} &= \sqrt{6} Q, & M_c &= \frac{2\sqrt{6} Q}{3}, \\ P_c &= \frac{1}{96\pi Q^2}, & T_c &= \frac{1}{3\sqrt{6}\pi Q}. \end{aligned} \quad (\text{G2})$$

They are obtained by imposing the criticality conditions

$$\frac{\partial P}{\partial r_h} = \frac{\partial^2 P}{\partial r_h^2} = 0, \quad \frac{\partial T}{\partial r_h} = \frac{\partial^2 T}{\partial r_h^2} = 0. \quad (\text{G3})$$

Using these reduced variables, we further obtain

$$\tilde{P}(\tilde{r}_h, \tilde{T}_0) = \frac{1 - 6\tilde{r}_h^2 + 8\tilde{r}_h^3 \tilde{T}_0}{3\tilde{r}_h^4}, \quad (\text{G4})$$

$$\frac{d\tilde{M}}{d\tilde{r}_h}(\tilde{r}_h, \tilde{T}_0) = \frac{-1 + 3\tilde{r}_h^2 + 4\tilde{r}_h^3 \tilde{T}_0}{6\tilde{r}_h^2}, \quad (\text{G5})$$

which no longer contain q explicitly, so the conclusions derived from them apply to arbitrary charge. The only remaining control parameter is \tilde{T}_0 . To ensure $\tilde{P}(\tilde{r}_h, \tilde{T}_0) \geq 0$ for all \tilde{r}_h , one must have $\tilde{T}_0 \geq \sqrt{2}/2$, while the first-order phase transition occurs only for $T_0 < T_c$, i.e., $\tilde{T}_0 < 1$. Thus the relevant range is $\tilde{T}_0 \in [\sqrt{2}/2, 1]$.

Within this interval, we numerically extract $r_{h,s}$ from $\tilde{P}(\tilde{r}_h, \tilde{T}_0)$ via the Maxwell equal-area construction, and obtain $r_{h,e}$ from the zero of $d\tilde{M}/d\tilde{r}_h$. The resulting curves are shown in Fig. 9. From this figure, one clearly sees that $r_{h,e} < r_{h,s}$ for all \tilde{T}_0 in the allowed range. Equivalently, the zero of dr_{ps}/dr_h always lies to the left of $r_{h,s}$, demonstrating that the phase transition takes place on the increasing branch of $r_{\text{ps}}(r_h)$.

We now extend this conclusion to the ISCO case. From the criterion (3.17), i.e.,

$$\frac{dr_c}{dr_h} = -\frac{1}{\Gamma_\epsilon} \left(\frac{dM}{dr_h} \partial_M \Phi_\epsilon + \frac{dP}{dr_h} \partial_P \Phi_\epsilon \right), \quad (\text{G6})$$

we note that, if the term $dP/dr_h \partial_P \Phi_1$ is temporarily neglected, the zeros of $(dM/dr_h) \partial_M \Phi_1$ coincide with those of $(dM/dr_h) \partial_M \Phi_0$, since both are determined solely by dM/dr_h . Moreover, dr_{isco}/dr_h is an increasing function of r_h in a neighborhood of the zero. Restoring $dP/dr_h \partial_P \Phi_1$ then adds a positive contribution $-(1/\Gamma_1) dP/dr_h \partial_P \Phi_1 > 0$, which lifts the curve and shifts the zero of dr_{isco}/dr_h to smaller r_h . Consequently, the extremum of $r_{\text{isco}}(r_h)$ lies to the left of that of

$r_{\text{ps}}(r_h)$, and hence also to the left of $r_{h,s}$, so the phase transition again occurs on the increasing branch of $r_{\text{isco}}(r_h)$.

Therefore, under the isothermal constraint, although $r_c(r_h)$ of the four-dimensional RN-AdS black hole is globally non-monotonic, it remains locally monotonic within the phase transition region, thereby preserving the discontinuous jump across the phase transition.

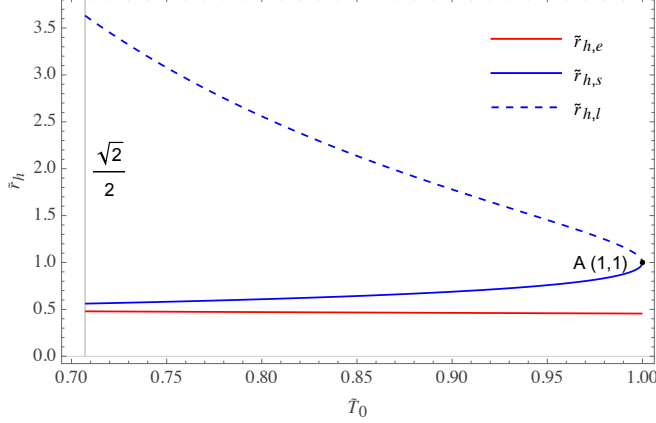


FIG. 9. Plots of $\tilde{r}_{h,e}$, $\tilde{r}_{h,s}$, and $\tilde{r}_{h,l}$ as functions of \tilde{T}_0 . The curves $\tilde{r}_{h,s}$ and $\tilde{r}_{h,l}$ intersect at point A, where $r_{h,s} = r_{h,l} = r_{h,c}$.

[1] J. M. Bardeen, B. Carter, and S. W. Hawking, The four laws of black hole mechanics, *Commun. Math. Phys.* **31**, 161 (1973).

[2] J. D. Bekenstein, Black holes and entropy, *Phys. Rev. D* **7**, 2333 (1973).

[3] J. D. Bekenstein, Generalized second law of thermodynamics in black hole physics, *Phys. Rev. D* **9**, 3292 (1974).

[4] S. W. Hawking, Particle creation by black holes, *Commun. Math. Phys.* **43**, 199 (1975).

[5] A. Strominger and C. Vafa, Microscopic origin of the Bekenstein-Hawking entropy, *Phys. Lett. B* **379**, 99 (1996).

[6] J. M. Maldacena, The large N limit of superconformal field theories and supergravity, *Adv. Theor. Math. Phys.* **2**, 231 (1998).

[7] E. Witten, Anti de Sitter space and holography, *Adv. Theor. Math. Phys.* **2**, 253 (1998).

[8] C. Niu, Y. Tian, and X.-N. Wu, Critical phenomena and thermodynamic geometry of Reissner-Nordström-anti-de Sitter black holes, *Phys. Rev. D* **85**, 024017 (2012).

[9] D. Kubiznak and R. B. Mann, P-V criticality of charged AdS black holes, *J. High Energy Phys.* **07** (2012) 033.

[10] S. Gunasekaran, R. B. Mann, and D. Kubiznak, Extended phase space thermodynamics for charged and rotating black holes and Born-Infeld vacuum polarization, *J. High Energy Phys.* **11** (2012) 110.

[11] R.-G. Cai, L.-M. Cao, L. Li, and R.-Q. Yang, P-V criticality in the extended phase space of Gauss-Bonnet black holes in AdS space, *J. High Energy Phys.* **09** (2013) 005.

[12] S.-W. Wei and Y.-X. Liu, Critical phenomena and thermodynamic geometry of charged Gauss-Bonnet AdS black holes, *Phys. Rev. D* **87**, 044014 (2013).

[13] P. Cheng, S.-W. Wei, and Y.-X. Liu, Critical phenomena in the extended phase space of Kerr-Newman-AdS black holes, *Phys. Rev. D* **94**, 024025 (2016).

[14] S.-W. Wei, B. Liang, and Y.-X. Liu, Critical phenomena and chemical potential of a charged AdS black hole, *Phys. Rev. D* **96**, 124018 (2017).

[15] R.-B. Wang, S.-J. Ma, L. You, Y.-C. Tang, Y.-H. Feng, X.-R. Hu, and J.-B. Deng, Thermodynamics of AdS-Schwarzschild-like black hole in loop quantum gravity, *Eur. Phys. J. C* **84**, 1161 (2024).

[16] L. You, R.-B. Wang, Y.-C. Tang, J.-B. Deng, and X.-R. Hu, Thermal chaos of quantum-corrected-AdS black hole in the extended phase space, *Eur. Phys. J. C* **84**, 1133 (2024).

[17] K. Akiyama *et al.* (Event Horizon Telescope Collaboration), First M87 Event Horizon Telescope results. VI. The shadow and mass of the central black hole, *Astrophys. J. Lett.* **875**, L6 (2019).

[18] K. Akiyama *et al.* (Event Horizon Telescope Collaboration), First Sagittarius A* Event Horizon Telescope results. I. The shadow of the supermassive black hole in the center of the Milky Way, *Astrophys. J. Lett.* **930**, L12 (2022).

[19] S.-W. Wei and Y.-X. Liu, Photon orbits and thermodynamic phase transition of d -dimensional charged AdS black holes, *Phys. Rev. D* **97**, 104027 (2018).

[20] S.-W. Wei, Y.-X. Liu, and Y.-Q. Wang, Probing the relationship between the null geodesics and thermodynamic phase transition for rotating Kerr-AdS black holes, *Phys. Rev. D* **99**, 044013 (2019).

[21] Y.-M. Xu, H.-M. Wang, Y.-X. Liu, and S.-W. Wei, Photon sphere and reentrant phase transition of charged Born-Infeld-AdS black holes, *Phys. Rev. D* **100**, 104044 (2019).

[22] A. Naveena Kumara, C. L. Ahmed Rizwan, S. Punacha, K. M. Ajith, and M. S. Ali, Photon orbits and thermodynamic

phase transition of regular AdS black holes, *Phys. Rev. D* **102**, 084059 (2020).

[23] Y.-Z. Du, H.-F. Li, F. Liu, and L.-C. Zhang, Photon orbits and phase transition for non-linear charged anti-de Sitter black holes, *J. High Energy Phys.* 01 (2023) 137.

[24] S.-J. Yang, S.-P. Wu, S.-W. Wei, and Y.-X. Liu, Deciphering black hole phase transitions through photon spheres, *Sci. China Phys. Mech. Astron.* **68**, 120412 (2025).

[25] M. Zhang, S.-Z. Han, J. Jiang, and W.-B. Liu, Circular orbit of a test particle and phase transition of a black hole, *Phys. Rev. D* **99**, 065016 (2019).

[26] M. Zhang and M. Guo, Can shadows reflect phase structures of black holes?, *Eur. Phys. J. C* **80**, 790 (2020).